Biphoton generation in a two-level atomic ensemble

Jianming Wen,[1,*] Shengwang Du,[2] and Morton H. Rubin[1]
[1]*Physics Department, University of Maryland, Baltimore County, Baltimore, Maryland 21250*
[2]*Edward L. Ginzton Laboratory, Stanford University, Stanford, California 94305*
(Received 30 October 2006; published 19 March 2007)

We have theoretically studied the space-time entangled biphoton state generated from a two-level atomic system. In the photon counting measurement, the two-photon coincidence counting rate is a damped oscillation. The oscillation period is determined by the effective Rabi frequency and the damping rate is determined by the linewidth of the inhomogeneous-broadened ground state and the dipole dephasing rate. In an optical-pathway-balanced configuration, the two-photon temporal correlation shows an antibunching effect which corresponds to the interference between two types of nonlinear four-wave mixing processes occurring in such a two-level system. The visibility of the normalized second-order quantum coherence function $g^{(2)}(\tau)$ increases along with the increase of the effective Rabi frequency, but has an upper limit at 45%. We find agreement between the theory and the experiments [P. Kolchin *et al.*, Phys. Rev. Lett. **97**, 113602 (2006); S. Du, J.-M. Wen, M. H. Rubin, and G. Y. Yin, *ibid* **98**, 053601 (2007)].

DOI: 10.1103/PhysRevA.75.033809 PACS number(s): 42.50.Dv, 42.65.Lm, 42.65.An, 32.80.−t

I. INTRODUCTION

Since the seminal work of Einstein, Podolsky, and Rosen [1], entangled states of two or more quantum particles has become the heart of many major paradoxes associated with the interpretation of quantum mechanics [2,3]. Entangled pure states are states of $N \geqslant 2$ particles that cannot be written as products of single-particle states. The importance of these states has been known since the earliest days of quantum theory [1–3]. Entangled photon pairs are not only of interest in themselves, but have many potential applications ranging from quantum computing and communication [4], imaging [5], lithography [6], optical measurement [7], to spectroscopy [8].

Conventionally, a powerful technique for generating paired photons is spontaneous parametric down conversion (SPDC), in which a pump laser drives the atomic oscillators in a noncentrosymmetric crystal into a nonlinear regime, and then two down-converted beams are radiated by these oscillations. SPDC has been extensively studied in both theory and experiment for more than two decades [9,10]. Recently, generation of paired photons by using electromagnetically induced transparency (EIT) [11] has attracted a great deal of attention in both experiment and theory [12–17]. Compared with the standard SPDC tool, this source of correlated photons has such benefits such as narrow spectrum, high conversion efficiency, long coherence time, and coherence length.

It has been known for a long time that four-wave parametric interactions in a strongly driven two-level system [18] may produce correlated photons [19,20]. However, experiments done in either an atomic beam [19] or a room temperature cell [20] have very low generation rate and require very long measurement time. In this paper, we present a detailed theoretical study of biphoton generation from a two-level system using magneto-optically trapped cold ^{87}Rb atomic ensemble. A direct experimental comparison between such a two-level atomic biphoton emitter and EIT-based multilevel system has been presented in a recent publication [15]. In the presence of a retroreflected pump beam, entangled photon pairs are spontaneously radiated into opposing single-mode fibers (SMF) and detected by photodetectors D1 and D2 (see Fig. 1). Since the nonlinearity is very small, this allows us to approximate the output state at the output surface(s) of the medium in the two-photon limit by the time-dependent perturbation theory. Here we emphasize the two-photon amplitude which is of importance in most of the two-photon optics. We found that in the photon counting measurement, the feature of the two-photon coincidence counting rate is a damped Rabi oscillation, which is in agreement with the experimental results. The oscillation period is determined by the effective Rabi frequency Ω_e and the damping rate is determined by the linewidth γ_g of the inhomogeneous-broadened ground state and the dipole dephasing rate γ_2. In an optical-pathway-balanced experiment, photon antibunching [21] appears. In the two-photon amplitude picture, this antibunching effect can be interpreted as the interference between two types of four-wave mixing processes (see Fig. 2) which occur in a two-level system. The visibility of the second-order quantum coherence function $g^{(2)}(\tau)$ increases along with the increase of the effective Rabi frequency, but has an upper limit of 45%. The comparison between theory and experiment shows a good agreement. In

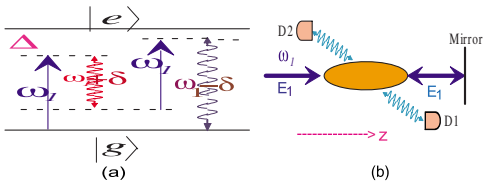

FIG. 1. (Color online) (a) Four-wave mixing in a two-level system. In the presence of a retroreflected pump beam at frequency ω_1, the two-level atoms scatter light into correlated fields at the frequencies $\omega_1+\delta$ and $\omega_1-\delta$. The pump detuning is $\Delta=\omega_1-\omega_{eg}$. (b) In the photon counting measurement, detectors D1 and D2 are applied to collect paired photons propagating in opposite directions.

*Electronic address: jianm1@umbc.edu

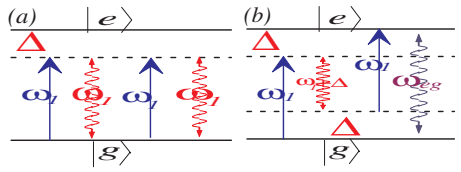

FIG. 2. (Color online) (a) Resonance around $\delta=0$. In such a case, the generated beams are scattered at the same frequency ω_1 as the pump laser. (b) Resonances around $\delta=\pm\Omega_e$. In such a case, the pump laser creates two *virtual states*, shown as dashed lines, one at an energy $\hbar\omega_1$ above the ground state $|g\rangle$ and the other at an energy $\hbar\omega_1$ below the excitation state $|e\rangle$. Photons from the pump laser will be inelastically scattered at two frequencies $\omega_1+\Delta$ and ω_{eg}, as shown by wave arrows.

this paper, we focus on the two-photon temporal correlation.

The paper is organized as follows. In Sec. II, the optical response of the two-level system is formulated in quantum theory. The first-order linear susceptibility χ carries the information about the dispersion profile and transmission spectrum of such a two-level medium. The third-order nonlinear susceptibility $\chi^{(3)}$ determines the parametric conversion coefficient and also indicates two kinds of physical processes which occur in this four-wave mixing. In Sec. III, the two-photon state at the output surface(s) of the medium is obtained by the first-order perturbation theory. The bandwidth of the biphoton is determined by both the phase matching and linewidths of triplet resonances in such a two-level system. In Sec. IV, theoretical analysis shows that the two-photon temporal correlation is a damped Rabi oscillation. Based on the normalized second-order quantum coherence function $g^{(2)}(\tau)$, the visibility is studied and its upper limit is found to be below 45%. This is further confirmed by comparing the theoretical results with the experimental data. In the Appendix, the calculation of the single-photon counting rate is provided.

II. OPTICAL RESPONSE OF A TWO-LEVEL SYSTEM

We consider a medium of identical two-level atoms or molecules initially in their ground state $|g\rangle$ [Fig. 1(a)], contained in a long thin cylindrical volume with length L and cross area A, and the average atomic density N. The idealized two-level atoms are separated by the atomic resonance frequency ω_{eg}. In the presence of a retroreflected pump beam, paired photons are spontaneously created and propagate into opposite directions. When the pump laser with frequency ω_1 is applied to atomic transition $|g\rangle\rightarrow|e\rangle$ with a detuning $\Delta=\omega_1-\omega_{eg}$, the response of the atomic system is driven to oscillate at the frequencies $\omega_3=\omega_1+\delta$ and $\omega_4=\omega_1-\delta$, shown as wavy arrows in Fig. 1(a). The character of this nonlinear process may be profoundly modified due to the strong intensity of the pump laser and, in such a case, perturbation theory is not sufficient to describe the interaction between the pump and medium. In the photon counting measurements [Fig. 1(b)], the photodetectors D1 and D2 are used to detect correlated photon pairs. For cold ^{87}Rb atoms with a typical temperature of 100 μK, the Doppler effect is small. Therefore, in the following discussions we consider an ideal system in which the Doppler effect will not be taken into account. In addition, the polarization of light is also not taken into account.

The dynamics of a single atom is described by the atomic operators, which at the initial time are given by

$$Q_{ij}(0)=|i\rangle\langle j| \quad (i,j=g \text{ or } e),$$

and satisfies the Heisenberg operator equation of motion in the dipole approximation

$$\dot{Q}_{ge}=-(i\omega_{eg}+\gamma_2)Q_{ge}-id_{eg}\tilde{E}Q_z+\mathcal{F}_{ge}, \tag{1}$$

$$\dot{Q}_{ee}=-(Q_{ee}-Q_{ee}^{eq})\gamma_e+2\,\mathrm{Im}[d_{ge}\tilde{E}^*Q_{ge}]+\mathcal{F}_{ee}, \tag{2}$$

$$\dot{Q}_{gg}=-(Q_{gg}-Q_{gg}^{eq})\gamma_g-2\,\mathrm{Im}[d_{ge}\tilde{E}^*Q_{ge}]+\mathcal{F}_{gg}, \tag{3}$$

where $d_{eg}=\langle e|\mathbf{d}|g\rangle/\hbar$ is the dipole matrix element divided by $\hbar$, and $\omega_{eg}=\omega_e-\omega_g$ is the atomic transition frequency between states $|e\rangle$ and $|g\rangle$. $Q_z=Q_{ee}-Q_{gg}$ describes the population inversion and $Q^{eq}=Q_{ee}^{eq}-Q_{gg}^{eq}$ is the equilibrium population inversion in the absence of the optical fields. γ_e and γ_g are the population relaxation rate of the excitation state and the linewidth of the inhomogeneous-broadened ground state, and $\gamma_2=1/T_2$ is the dipole dephasing rate, respectively. $\mathcal{F}_{\alpha\beta}$ are the quantum Langevin noise operators. Since these Langevin noise operators introduce the unpaired photons which are not of interest here, they will be ignored from now on [22]. $\tilde{E}(t)$ is the positive frequency total field operator

$$\tilde{E}(t)=E(t)e^{-i\omega_1 t}=[E_1+E_3^{(+)}e^{-i\delta t}+E_4^{(+)}e^{i\delta t}]e^{-i\omega_1 t}, \tag{4}$$

where E_1 represents the slowly varying amplitude of classical pump field, and $E_3^{(+)}$ and $E_4^{(+)}$ are field operators of generated beams. In order to eliminate the fast oscillating phase terms in Eqs. (1)–(3), we introduce the following transformation

$$Q_{ge}(t)=\sigma(t)e^{-i\omega_1 t}. \tag{5}$$

Now Eqs. (1)–(3) become

$$\dot{\sigma}=(i\Delta-\gamma_2)\sigma-id_{eg}E(Q_{ee}-Q_{gg}), \tag{6}$$

$$\dot{Q}_{ee}=-(Q_{ee}-Q_{ee}^{eq})\gamma_e+2\,\mathrm{Im}[d_{ge}E^*\sigma], \tag{7}$$

$$\dot{Q}_{gg}=-(Q_{gg}-Q_{gg}^{eq})\gamma_g-2\,\mathrm{Im}[d_{ge}E^*\sigma]. \tag{8}$$

Equations (6)–(8) cannot be readily solved exactly for the field given in Eq. (4). Instead, we will adopt the treatment in Ref. [18] and try to find a solution keeping all orders to pump field E_1 while maintaining the lowest order in $E_{3,4}$ of the weak fields. Therefore, the steady-state solution of Eqs. (6)–(8) is required to be of the form

$$\sigma=\sigma_0+\sigma_3e^{-i\delta t}+\sigma_4e^{i\delta t}, \quad Q_{ee}=Q_e+Q_{e3}e^{-i\delta t}+Q_{e3}^{\dagger}e^{i\delta t},$$

$$Q_{gg}=Q_g+Q_{g3}e^{-i\delta t}+Q_{g3}^{\dagger}e^{i\delta t}, \tag{9}$$

where σ_0, Q_e, and Q_g are the solution for the case in which only the pump field E_1 is present, while the other terms are

assumed to be small such that $|\sigma_3|,|\sigma_4| \ll |\sigma_0|$ and $|Q_{e3}| \ll |Q_e|$, $|Q_{g3}| \ll |Q_g|$. In addition, we set $Q_0 = Q_e - Q_g$, $Q_3 = Q_{e3} - Q_{g3}$, and $Q_3^\dagger = Q_{e3}^\dagger - Q_{g3}^\dagger$.

We next substitute the trial solution (9) into Eqs. (6)–(8) and look at the terms with the same time dependence. As stated above, we will drop any term that contains the product of more than one small quantity. Then after some algebra, we have

$$Q_0 = \frac{\Delta^2 + \gamma_2^2}{\Delta^2 + \gamma_2^2 + \frac{\gamma_2}{2}\left(\frac{1}{\gamma_e} + \frac{1}{\gamma_g}\right)|\Omega_1|^2} Q^{eq}, \quad \sigma_0 = \frac{d_{eg} E_1 Q_0}{\Delta + i\gamma_2}, \tag{10}$$

$$Q_3 = -\frac{2|d_{ge}|^2 Q_0(\delta + 2i\gamma_2)}{D(\delta)}\left[\frac{\delta - \Delta + i\gamma_2}{\Delta - i\gamma_2} E_1^* E_3^{(+)} - \frac{\delta + \Delta + i\gamma_2}{\Delta + i\gamma_2} E_1 E_4^{(-)}\right], \tag{11}$$

$$\sigma_3 = \frac{d_{eg}(E_1 Q_3 + E_3^{(+)} Q_0)}{\Delta + \delta + i\gamma_2}, \tag{12}$$

$$\sigma_4 = \frac{d_{eg}(E_1 Q_3^\dagger + E_4^{(+)} Q_0)}{\Delta - \delta + i\gamma_2}, \tag{13}$$

where

$$D(\delta) = \left[\frac{(\delta + i\gamma_e)(\delta + i\gamma_g)}{\delta + i(\gamma_g + \gamma_e)/2}\right](\delta + \Delta + i\gamma_2)(\delta - \Delta + i\gamma_2) - |\Omega_1|^2(\delta + i\gamma_2) = -D^*(-\delta). \tag{14}$$

Here we have introduced the Rabi frequency $\Omega_1 = 2d_{eg}E_1$. The physics of Eqs. (10)–(13) can be understood as follows. Equation (10) describes the optical response of the atoms to the pump field. σ_0 characterizes the linear Rayleigh scattering of the pump and will result in the background noise in the coincidence counting measurement. Without the pump beam, $Q_0 = Q^{eq}$ as we expected. Equations (11) and (12) together show the optical response to the generated ω_3 field. As we shall see below, among those terms two contribute to the effective linear susceptibility and the third one is for the third-order nonlinear susceptibility which is the quantity of interest in the paired photon generation. On the right-hand side (RHS) of Eq. (11), the first term corresponds to the Rayleigh-wing scattering at frequency ω_3 and the second term to the correlated photon generation. On the RHS of Eq. (12), the first term is the nonlinear optical response to the generated ω_3 field while the second term is the linear Rayleigh scattering of the ω_3 field. Similarly, $Q_3^\dagger$ plus Eq. (13) gives the information of optical response to the ω_4 field. Q_3 (and consequently σ_3 and σ_4) shows a resonance whenever the pump beam is tuned to the line center so that $\Delta = 0$, or whenever the real part of the function $D(\delta)$ gives a zero. In the limit $|\Omega_1| \to 0$, i.e., the weak-optical-excitation case, the zeros of $D(\delta)$ occur near $\delta = 0, \pm\Delta$. In general, $|\Omega_1|^2$ is not small and the full form of Eq. (14) should be kept. To determine its resonance structure, we write $D(\delta)$ in terms of its real and imaginary parts and assume $\gamma_e \gg \gamma_g$ so that $(\delta + i\gamma_e)(\delta + i\gamma_g)/[\delta + i(\gamma_e + \gamma_g)/2] \approx (\delta + i\gamma_g)$. Solving $\mathrm{Re}\, D(\delta) = 0$ gives a triplet of resonances occurring at

$$\delta = 0, \quad \delta = \pm\sqrt{\Omega_e^2 + \gamma_2^2 + 2\gamma_g\gamma_2},$$

where we have introduced the effective Rabi frequency $\Omega_e = \sqrt{\Delta^2 + |\Omega_1|^2}$. To further understand the physical processes behind $D(\delta)$, we assume $\Omega_e \gg (\gamma_e, \gamma_g, \gamma_2)$. In such a limit, the three resonances occur at $\delta = 0, \pm\Omega_e$ and they are well separated. Near the (central) resonance at $\delta = 0$, $D(\delta)$ can be approximated as

$$D(\delta) = -\Omega_e^2(\delta + i\Gamma_0), \quad \Gamma_0 = \frac{\Delta^2}{\Omega_e^2}\gamma_g + \frac{|\Omega_1|^2}{\Omega_e^2}\gamma_2. \tag{15}$$

Γ_0 represents the width of this resonance. In the case of weak optical pumping, i.e., $|\Omega_1| \ll \Delta$, Γ_0 approaches the linewidth γ_g of the inhomogeneous-broadened ground state while in the case of strong optical excitation, i.e., $|\Omega_1| \gg \Delta$, Γ_0 reaches the dipole dephasing rate γ_2. In the same way, near the (sideband) resonances at $\delta = \pm\Omega_e$, $D(\delta)$ can be approximated as

$$D(\delta) = 2\Omega_e^2(\delta \mp \Omega_e + i\Gamma), \quad \Gamma = \frac{|\Omega_1|^2}{\Omega_e^2}\left(\frac{\gamma_g + \gamma_2}{2}\right) + \frac{\Delta^2}{\Omega_e^2}\gamma_2. \tag{16}$$

The sidebands have the same linewidth Γ. As seen from Eq. (16), Γ goes to γ_2 in the weak-optical-excitation limit, while it approaches $(\gamma_g + \gamma_2)/2$ when $|\Omega_1| \gg \Delta$.

Two types of physical processes behind $D(\delta)$ are illustrated in Fig. 2. When the (central) resonance occurs around $\delta = 0$, the generated beams have the same central frequencies as the pump beam, as shown in Fig. 2(a). In this case, the correlated photon pairs are generated due to the absorption of a pair counter-propagating pump photons as required by the phase matching conditions. The spontaneously emitted paired photons propagate into opposite directions. This leads to the photon bunching effect as discovered by Hanbury-Brown and Twiss [23]. When the resonances appear around $\delta = \pm\Omega_e$, i.e., sideband generation as depicted in Fig. 2(b), the pump laser creates two *virtual states*, one at an energy $\hbar\omega_1$ above the ground state $|g\rangle$ and the other at an energy $\hbar\omega_1$ below the excitation state $|e\rangle$. The central frequencies of generated fields which are peaked around $\omega_1 + \Delta$ are due to the inelastic scattering of the pump beam. The two types of physical processes demonstrated in Fig. 2 occur in four-wave mixing in a two-level system with the same coefficient. As we shall see in Sec. IV A, these two kinds of parametric processes may destructively interfere with each other and result in the photon antibunching effect in a two-photon coincidence counting measurement.

Now let us look at the optical response of the atomic dipoles at frequencies $\omega_1 \pm \delta$. We are interested in the susceptibilities. The slowly varying amplitudes of polarization operators for an ensemble are given by $\mathcal{P}(\omega_3) = N\hbar d_{ge}\sigma_3$ and $\mathcal{P}(\omega_4) = N\hbar d_{ge}\sigma_4$ with the atomic density N. The relationship between the polarization and the susceptibility is $\mathcal{P} = \epsilon_0\chi E$

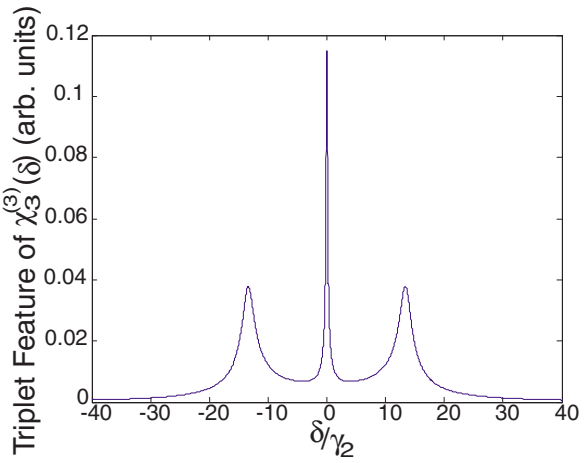

FIG. 3. (Color online) Triplet resonances shown in $|\chi_3^{(3)}(\delta)|$. In the simulation, the parameters were chosen as $\gamma_g/\gamma_2=0.087$, $|\Delta|/\gamma_2=13.3$, and $|\Omega_1|/\gamma_2=1.38$.

$+\epsilon_0\chi^{(3)}EEE$, where χ is the effective linear susceptibility and $\chi^{(3)}$ is the third-order nonlinear susceptibility [18]. By using Eqs. (10)–(13), one can find that

$$\chi_3(\delta)=\frac{N\hbar|d_{ge}|^2Q_0}{\epsilon_0(\Delta+\delta+i\gamma_2)}\left[1-\frac{|\Omega_1|^2(\delta+2i\gamma_2)(\delta-\Delta+i\gamma_2)}{2D(\delta)(\Delta-i\gamma_2)}\right], \tag{17}$$

$$\chi_3^{(3)}(\delta)=\frac{2N\hbar|d_{ge}|^4Q_0(\delta+2i\gamma_2)}{\epsilon_0D(\delta)(\Delta+i\gamma_2)}, \tag{18}$$

$$\chi_4(\delta)=\chi_3(-\delta), \tag{19}$$

$$\chi_4^{(3)}(\delta)=\chi_3^{(3)}(-\delta). \tag{20}$$

Equations (19) and (20) show the symmetry between the optical responses to the ω_3 and ω_4 fields. The effective linear susceptibilities χ_3 and χ_4 determine the dispersion profile and transmission spectrum of the weak fields ω_3 and ω_4 crossing through the medium, respectively. It is known that the natural spectral width of paired photon is governed by the dispersion, which is determined by the effective linear susceptibility as shall be seen below. The third-order nonlinear susceptibilities $\chi_3^{(3)}$ and $\chi_4^{(3)}$ not only control the parametric conversion efficiency of paired photons generation but also play an important role in the two-photon amplitude (or wave packet). It is easy to verify that $\chi^{(3)}\propto 1/\Omega_e^2\Delta$ in the large pump-detuning limit. On the RHS of Eqs. (17) and (19), the first term corresponds to the linear Rayleigh scattering of the ω_3 and ω_4 fields and the second term to the nonlinear Rayleigh scattering. As seen from Eqs. (17) and (19), the effective linear optical responses χ at frequencies $\omega_1\pm\delta$ come from two contributions. The first one corresponds to the dc part of the population inversion Q_0 because of the linear Rayleigh scattering at frequencies $\omega_1\pm\delta$. The second one is the result of population oscillations, which will give the background of Rayleigh-wing scattering. In Fig. 3, the feature of triplet resonances is shown by plotting $|\chi_3^{(3)}(\delta)|$ as a function of δ/γ_2. The parameters are chosen as $\gamma_g/\gamma_2=0.087$, $|\Delta|/\gamma_2=13.3$, and $|\Omega_1|/\gamma_2=1.38$. It is obvious that the central component is much narrower than two sidebands and two sidebands are located around $\pm\Delta$, as discussed above. It is found that when γ_g increases, the central peak decreases, meanwhile its bandwidth increases.

Before proceeding with the discussion, it is necessary to look at the phase matching of such a four-wave mixing in a two-level system. The nonlinear optical response of the medium as described by Eqs. (17)–(20) will, of course, influence the propagation dynamics of the weak fields at frequencies $\omega_1\pm\delta$. It is useful to write the linear susceptibilities as their real and imaginary parts $\chi=\chi'+i\chi''$. The propagation constant of two weak fields within the medium is given by $k_{3,4}=(\omega_1\pm\delta)/v_{3,4}$. Here $v_{3,4}$ are group velocities of two weak fields propagating through the system, which is defined by $v=c/[n+\omega(dn/d\omega)]$. $n(\omega)$ is the refractive index experienced by each photon and is defined as $n=\sqrt{1+\chi'}$. Therefore, the group velocity can be written as

$$v_{3,4}=\frac{c}{1+\frac{\omega_1}{2}\frac{d\chi'}{d\delta}\frac{d\delta}{d\omega_{3,4}}}. \tag{21}$$

Combining Eq. (17) with Eq. (19) gives $v_3=v_4$, which is as expected in such a two-level system. In the counterpropagating geometrical scheme, the resulting wave-vector mismatch is

$$\Delta k=k_3-k_4=\frac{2\delta}{v_3}. \tag{22}$$

In the derivation of Eq. (22) we have expanded the propagation constants k_3 and k_4 to first order in δ using the dispersion relations, and also used $v_3=v_4$. However, in the copropagating case, the expansion of $k_{3,4}$ must be carried out up to the second order, i.e., the dispersion of group velocity. The bandwidth due to the group delay can be estimated from Eq. (22) as $\Delta\omega_\Phi\sim v_3/2L$. As mentioned above, the transmission profile is determined by χ''. The bandwidth, which is allowed to propagate, is then given by $\Delta\omega_{tr}=\sqrt{c/\omega_pL[d^2\chi''/d\delta^2]}$.

Before we move to the next section, let us look at one example. Consider the ^{87}Rb D2 line transition with the parameters $\Omega_1=26$ MHz, $\Delta=2\pi\times40$ MHz, $\gamma_e=2\pi\times6$ MHz, $\gamma_2=2\pi\times3$ MHz, $\gamma_g=2\pi\times0.26$ MHz, $N=2\times10^{17}$ atoms/m^3, and $L=1.5$ mm. Then, the refractive index $n\approx1$ and the group velocity $v=3.55\times10^5$ m/s. The bandwidth resulting from the phase mismatching (or the dispersion) is $\Delta\omega_\Phi=0.12$ GHz and the bandwidth due to the transmission profile takes the value of $\Delta\omega_{tr}=0.44$ GHz. The linewidths of the triplet resonances are 18.8 MHz (sidebands) and 1.61 MHz (central component). As we see, within this range, the two-photon bandwidth is mainly determined by the linewidths of triplet structure instead of the transmission bandwidth or phase mismatching.

III. TWO-PHOTON STATE IN A TWO-LEVEL SYSTEM

In this section we will formulate the two-photon state generated from such a two-level atomic ensemble. In the

interaction picture the effective Hamiltonian is given by

$$\mathcal{H}_{\text{eff}} = \epsilon_0 \int_V d^3 r \chi_3^{(3)} E_1^{(+)} E_2^{(+)} E_3^{(-)} E_4^{(-)} + \text{H.c.}, \tag{23}$$

where V is the interaction volume illuminated by the retroreflected pump beam and H.c. means the Hermitian conjugate. The electromagnetic fields of the output beams are given by the quantized fields

$$E_3^{(+)} = \sum_{\vec{k}_3} E_3 a_{\vec{k}_3} e^{i(\vec{k}\cdot\vec{r}-\omega_3 t)}, \quad E_4^{(+)} = \sum_{\vec{k}_4} E_4 a_{\vec{k}_4} e^{-i(\vec{k}\cdot\vec{r}+\omega_4 t)}, \tag{24}$$

where $E_j = i\sqrt{\hbar\omega_j/2\epsilon_0 n_j^2 V_Q}$, V_Q is the quantization volume. The retroreflected pump beam is taken to be a classical plane wave,

$$E_1^{(+)} = E_1 e^{i(k_1 z-\omega_1 t)}, \quad E_2^{(+)} = E_1 e^{-i(k_1 z+\omega_1 t+\varphi)}, \tag{25}$$

where φ is the phase shift coming from the optical pathways. For simplicity we set $\varphi = 2m\pi$, where m is an integer. The z direction is assumed to be parallel to the pump longitudinal propagation [see Fig. 1(b)]. In writing the Hamiltonian (23) we have ignored the reflections from the system surfaces and further we made the rotating-wave approximation.

Since the nonlinearity is very small, the initial state of the generated photon pairs can be found from the first-order perturbation theory in the interaction picture. The calculation of the state vector to first order in perturbation theory gives

$$|\Psi\rangle = |0\rangle - \frac{i}{\hbar}\int_{-\infty}^{\infty} dt \mathcal{H}_{\text{eff}}|0\rangle = |0\rangle + \sum_{\vec{k}_3}\sum_{\vec{k}_4} F(\vec{k}_3,\vec{k}_4) a_{\vec{k}_3}^{\dagger} a_{\vec{k}_4}^{\dagger}|0\rangle, \tag{26}$$

where $\vec{k}_3$ and $\vec{k}_4$ are evaluated inside the medium and $a_{\vec{k}_j}^{\dagger}$ is the creation operator at the output surface of the medium associated with the wave vector $\vec{k}_j$. In general, $|\Psi\rangle$ will be a superposition of the vacuum state $|0\rangle$ and states with many numbers of pairs of photons. On the RHS of Eq. (26), the first term is just the vacuum state which is not of interest, while the second term is called the two-photon state. F is the spectral function, which is given by

$$F(\vec{k}_3,\vec{k}_4) = \beta\delta(2\omega_1 - \omega_3 - \omega_4)\Phi(\Delta kL)H(\vec{\alpha}_3,\vec{\alpha}_4,\vec{\rho}). \tag{27}$$

For the detailed derivation of the spectral function F, one may follow the analysis given in Ref. [9]. The z integral from $-L$ to 0 over the length of the medium gives $\Phi(\Delta kL)$,

$$\Phi(\Delta kL) = \frac{1 - e^{-i\Delta kL}}{i\Delta kL}, \tag{28}$$

where $\Delta k = k_3 - k_4$ is given in Eq. (22). The integral over the area A of the intersection of the beam cross section and the medium gives

$$H(\vec{\alpha}_3,\vec{\alpha}_4,\vec{\rho}) = \frac{1}{A}\int_A d^2\rho e^{-i(\vec{\alpha}_3+\vec{\alpha}_4)\cdot\vec{\rho}}, \tag{29}$$

where we assumed that A is independent of z. The time integral gives the Dirac δ function, which states the energy conservation. In Eq. (27),

$$\beta = i\pi\chi_3^{(3)} E_1^2 \omega_1, \tag{30}$$

which is the parametric gain index for perfect phase matching. β can be taken as a constant if it is sufficiently slowly varying over the bandwidth of the parametric process. In the above derivations, we have assumed that the retroreflected pump beam is spatial constant over the interaction cross area A. To simplify the calculations, we also made an additional approximation that the cross section of the laser beam is large enough so that diffraction effects can be ignored. $\vec{\alpha}_3$ and $\vec{\alpha}_4$ are transverse mode vectors, respectively. $\vec{\rho}$ is in the transverse plane normal to the longitudinal axis z and is evaluated at the output surfaces of the medium.

Equation (28) is called the longitudinal detuning function, which carries the information of phase mismatch in the longitudinal direction over the entire medium. The natural spectral width of the two-photon state may be determined by this longitudinal detuning function. Equation (29) is called the transverse detuning function, which contains the information of momentum conservation in the transverse direction. For small emission angles and short effective-interaction-length (L_{eff}) medium (i.e., $L_{\text{eff}} \tan\theta \ll \kappa$, κ is a typical width in the transverse plane), the function $\Phi(\Delta kL)$ is close to unity when $H(\vec{\alpha}_3,\vec{\alpha}_4,\vec{\rho})$ has a non-negligible value. Now $H(\vec{\alpha}_3,\vec{\alpha}_4,\vec{\rho})$ determines the two-photon state properties. However, if $L_{\text{eff}} \tan\theta \gg \kappa$, the properties of the two-photon state are mainly determined by the function $\Phi(\Delta kL)$. In the limit of a medium with infinite length and cross section, Φ and H both become δ functions. Combining with the energy-conservation δ function, they form perfect phase matching conditions: $2\omega_1 = \omega_3 + \omega_4$ and $\vec{k}_3 - \vec{k}_4 = 0$. The phase-matching conditions arise from the fact that the parametric process is a coherent process in which all parts of the medium contribute in phase. For the finite L, the wave-number condition is relaxed so that $|\Delta k|$ may vary over an interval of order $1/L$. However, it should be noted that the range of bandwidth of generated paired photons is also strongly determined by their linewidths as mentioned in Sec. II. The example examined in the previous section has shown that the allowed two-photon bandwidth is mostly determined by their resonance linewidths. In such a case, the longitudinal detuning function is close to unity and the properties of the biphoton are mainly determined by the optical response $\chi^{(3)}$. Therefore, in the two-photon coincidence measurement, the pattern should reflect this point, as discussed in the following section.

To simplify the following discussions, we further made another assumption that the cross section of the retroreflected pump beam is constant and large enough so that the transverse detuning function (29) becomes a δ function. In this paper, we focus on the temporal correlation of the two-photon state and the wave vectors are replaced by wave numbers.

IV. PHOTON COUNTING MEASUREMENT

In most experiments the two-photon correlation is the quantity of primary interest. To look at the two-photon properties from a two-level system, we start with a simple experiment of photon coincidence counting measurement [see Fig. 1(b)]. For completeness, the single-photon counting detection is provided in the Appendix. The polarization effect of the generated fields are not taken into account. For simplicity, suppose that detector D1 detects photons with frequency ω_3 while photons with frequency ω_4 fire detector D2.

The averaged two-photon coincidence counting rate is defined by

$$R_{cc} = \lim_{T\to\infty} \frac{1}{T}\int_0^T dt_a \int_0^T dt_b \langle \Psi | E_a^{(-)} E_b^{(-)} E_b^{(+)} E_a^{(+)} | \Psi \rangle M(t_a - t_b), \tag{31}$$

where the free-space electromagnetic fields $E_j^{(+)}$ $(j=a,b)$ are defined in analogy with Eq. (24) and they are evaluated at detector Dj's coordinates spatial position r_j and trigger time t_j. $M(t)$ is the coincidence window function, which is defined so that $M=1$ for $|t|<t_{cc}$ and it goes to zero rapidly for $|t|>t_{cc}$. For the experiment analyzed here t_{cc} is quite large and so we may take $M=1$. In Eq. (31) the detector efficiencies are implicitly assumed to be unity. It is most convenient to perform the calculations in the Heisenberg picture in which the state vector is the steady-state output at the surfaces of the medium.

Using Eq. (26), the fourth-order field correlation function in Eq. (31), which describes the joint detection probability, can be written as

$$\langle \Psi | E_a^{(-)} E_b^{(-)} E_b^{(+)} E_a^{(+)} | \Psi \rangle = |\langle 0 | E_b^{(+)} E_a^{(+)} | \Psi \rangle|^2 = |A_{12}(\tau_a, \tau_b)|^2, \tag{32}$$

where $\tau_j = t_j - r_j/c$ and r_j is the optical path from the output surface of the medium to the jth detector $(j=a,b)$. In the following we choose $r_a = r_b$, i.e., the balanced optical pathways, to simplify the analysis. The function $A_{12}(\tau)$ is referred as the *two-photon amplitude*, or for short the *biphoton*.

Consider the case that there are no filters placed in front of the detectors. By substituting Eq. (24) into Eq. (32), one obtains

$$A_{12}(\tau_1, \tau_2) = \sum_{k_a}\sum_{k_b} E_{k_a} E_{k_b} e^{-i(\omega_a \tau_1 + \omega_b \tau_2)} \langle 0 | a_{k_a} a_{k_b} | \Psi \rangle. \tag{33}$$

The discussion about the function of filters inserted in the system may follow the treatment analyzed in [9]. Next, using Eq. (26) we find

$$\langle 0 | a_{k_a} a_{k_b} | \Psi \rangle = \sum_{k_3}\sum_{k_4} F(k_3, k_4) \delta_{k_3 k_a} \delta_{k_4 k_b}. \tag{34}$$

Substituting this into Eq. (33) and evaluating the summations using the Kronecker δ, we have

$$A_{12}(\tau_1, \tau_2) = \sum_{k_3}\sum_{k_4} W_{k_3 k_4} \chi^{(3)} \delta(2\omega_1 - \omega_3 - \omega_4) \times \Phi(\Delta k z) e^{-i(\omega_3 \tau_1 + \omega_4 \tau_2)}. \tag{35}$$

The functions which vary slowly over the bandwidth of the beams have been grouped into $W_{k_3 k_4}$. Now converting the sums in Eq. (35) into integrals in the standard fashion,

$$\sum_{k_j} \to \frac{V_Q^{1/3}}{2\pi}\int \frac{dk_j}{d\omega_j} d\omega_j = \frac{V_Q^{1/3}}{2\pi}\int \frac{d\omega_j}{v_j}, \tag{36}$$

and using Eq. (22), the two-photon amplitude (35) becomes

$$A_{12}(\tau_1, \tau_2) = W e^{-i\omega_1 \tau_+} \int_{-\varpi_3}^{\varpi_4} d\delta \chi_3^{(3)}(\delta) \Phi\left(\frac{2\delta L}{v_3}\right) e^{-i\delta\tau_-}, \tag{37}$$

where $\tau_+ = \tau_1 + \tau_2$ and $\tau_- = \tau_1 - \tau_2$. ϖ_3 and ϖ_4 represent the lower and upper limits of the integral. In the above expression, we have absorbed all the slowly varying quantities into W and put it out of the integral. The limits on the integral may be taken to $\pm\infty$ since (1) the longitudinal detuning function Φ is peaked around $\delta=0$ and has a bandwidth of order $v_3/2L$, which is generally much smaller than ω_1 and (2) the linewidths of the triplet spectrum gives a much narrower bandwidth which control the profile of the biphoton. The integral in Eq. (37) is a Fourier transform of the longitudinal detuning function times the profile of the third-order nonlinear susceptibility. In general, the pattern of the two-photon amplitude is determined by both Φ and $\chi^{(3)}$. However, the narrower bandwidth resulting from either Φ or resonance linewidths will finally determine the feature of the two-photon correlation detection.

A. Narrow-band generation of paired photons

Let us consider the case of $\Delta\omega_\Phi \gg (\Gamma_0, \Gamma)$, i.e., narrow-band generation. In such a case, the two-photon amplitude Eq. (37) is mainly determined by the third-order nonlinear susceptibility profile, i.e.,

$$A_{12}(\tau_1, \tau_2) = W e^{-i\omega_1 \tau_+} \int_{-\varpi_3}^{\varpi_4} d\delta \chi_3^{(3)}(\delta) e^{-i\delta\tau_-}. \tag{38}$$

Considering $\Omega_e \gg (\gamma_e, \gamma_g, \gamma_2)$, the third-order nonlinear susceptibility Eq. (18) for the ω_3 photons may be expanded around the resonances ω_1 and $\omega_1 \pm \Omega_e$. Keeping the leading terms, one obtains

$$\chi_3^{(3)} = \frac{N\hbar |d_{ge}|^4 Q_0}{\epsilon_0 (\Delta + i\gamma_2)} \left[\frac{1}{(\delta + i\Gamma_0)(\delta + \Omega_e + i\Gamma)} + \frac{1}{(\delta + i\Gamma_0)(\delta - \Omega_e + i\Gamma)} \right]. \tag{39}$$

In the derivation of Eq. (39) we have applied Eqs. (15) and (16). The analysis about two types of four-wave mixing discussed in Sec. II is explicitly reflected in Eq. (39). In the square brackets, the first term indicates that the ω_3 field is resonant at angular frequencies ω_1 and $\omega_1 - \Omega_e$, while the

second term shows that the resonances occur at frequencies ω_1 and $\omega_1+\Omega_e$. These two processes destructively contribute to the total third-order nonlinear susceptibility $\chi_3^{(3)}$. One may check that in the large pump-detuning case, Eq. (39) is proportional to $1/\Omega_e^2\Delta$. Since the two terms in the square brackets in Eq. (39) contribute equally to the two-photon amplitude, we will keep only the first term by multiplying the factor 2. After this treatment, substituting Eq. (39) into Eq. (38) and extending the limitations of the integral to infinity, the two-photon amplitude now takes the form of

$$A_{12}(\tau_1,\tau_2)=\phi(\tau_+)\theta(\tau_-), \tag{40}$$

$$\phi(\tau_+)=We^{-i\omega_1\tau_+}, \tag{41}$$

$$\theta(\tau_-)=[e^{-\Gamma_0\tau_-}-e^{i\Omega_e\tau_-}e^{-\Gamma\tau_-}]\Pi(\tau_-). \tag{42}$$

Here $\Pi(\tau_-)$ is the Heaviside function. Again, all the constants and slowly varying terms have been absorbed into W and $W\propto 1/\Omega_e\Delta$. In the derivation we have used the assumption of $\Omega_e \gg (\gamma_e,\gamma_g,\gamma_2)$. The function $\theta(\tau_-)$ is a damped Rabi oscillation with the oscillation period $2\pi/\Omega_e$. If $\gamma_g \approx \gamma_2 \approx \gamma$, then $\Gamma=\Gamma_0$ and the function $\theta(\tau_-)$ has a simple expression

$$\theta(\tau_-)=(1-e^{i\Omega_e\tau_-})e^{-\gamma\tau_-}, \tag{43}$$

with a damping rate γ. The physics of Eq. (40) is understood as follows. Because the two-photon state is entangled, the biphoton cannot be factorized into a function of τ_1 times a function of τ_2. The factor $\phi(\tau_+)$ describes the fact that the pair can be generated at any time within the medium. If the pump laser were taken to be a wave packet rather than a plane wave, this term would also become a wave packet with the coherence length of the pump with the consequence that there would be a distribution of pump frequencies and wave numbers. The function $\theta(\tau_-)$ has two contributions, one from the central component of the triplet resonances [Fig. 2(a)] and the other from sidebands [Fig. 2(b)]. Each contribution has a Lorentzian line shape. By choosing the different γ_g, γ_e, γ_2, Δ, and Ω_1, the function $\theta(\tau_-)$ may exhibit photon bunching or antibunching effect. To see this, let us examine the two-photon coincidence counting rate.

By using Eqs. (40)–(42), the two-photon coincidence counting rate (31) now becomes

$$R_{cc}(\tau)=R_0[e^{-2\Gamma_0\tau}+e^{-2\Gamma\tau}-2\cos(\Omega_e\tau)e^{-(\Gamma_0+\Gamma)\tau}], \tag{44}$$

where R_0 is the grouped constant and we have denoted τ_- as τ. It should be noted that since the bandwidth of the biphoton is smaller than the spectral width of the detectors, the coincidence counting rate is simply the module-squared two-photon amplitude. Equation (44) shows a strong pairlike character and antibunching effect. The first term in Eq. (44) corresponds to the central-component correlation, the second one to sideband-sideband correlation, and the third appears as an interference between two previous terms. In a large-detuning or intense pump case, the triplet resonances may be well separated. Under such a situation, by choosing proper filters one can study the temporal correlations between photons emitted in given lines of the spectrum. If $\gamma_g \approx \gamma_2 \approx \gamma$, Eq. (44) reduces to a simple form,

$$R_{cc}(\tau)=2R_0[1-\cos(\Omega_e\tau)]e^{-2\gamma\tau}. \tag{45}$$

In the large-detuning and weak pump excitation case, the function R_{cc} vanishes as $\tau\to 0$, exhibiting the photon antibunching effect. As $\tau\to\infty$, R_{cc} also approaches to zero. The oscillation period is determined by the effective Rabi frequency Ω_e. The damping rate is equal to 2γ as shown in Eq. (45).

In the case of $\gamma_g \neq \gamma_2$, the whole damping rate will be determined by twice of $\min[\gamma_g,\gamma_2]$ [see Eq. (44)]. The observed antibunching effect is due to the destructive interference between the two types of four-wave mixing processes as discussed in Sec. II. Considering the realistic situation, the generated paired photons can trigger either of two detectors. The diagram of the two-photon coincidence counting rate is therefore expected to be a symmetric distribution. In Eq. (44), if $\Gamma_0 \ll \Gamma$ the two-photon correlation measurement will show a perfect photon antibunching effect. When the pump coincides with the atomic transition, in the weak coherent pumping case the two-photon correlation shows only the photon antibunching effect. There is no correlation between the central component and sidebands in the second-order coherence, but does show correlation at the third-order and higher-order coherence.

At a fixed position, the normalized second-order quantum coherence function depends only on the time difference $\tau=\tau_1-\tau_2$:

$$g^{(2)}(\tau)=\frac{\langle E_a^{(-)}(t)E_b^{(-)}(t+\tau)E_b^{(+)}(t+\tau)E_a^{(+)}(t)\rangle}{\langle E_a^{(-)}(t)E_a^{(+)}(t)\rangle\langle E_b^{(-)}(t+\tau)E_b^{(+)}(t+\tau)\rangle},$$

which is interpreted as the conditional probability that if a photon is detected at t the other one will be detected at $t+\tau$. Considering the two-photon generation in the two-level system, this normalized second-order quantum coherence function becomes

$$g^{(2)}=1+\frac{Rcc(\tau)}{R_R^2}. \tag{46}$$

Here R_R represents the linear Rayleigh scattering rate for one photodetector. For a single-transverse-mode fiber, in the case of $\Delta \gg (\gamma_e,\gamma_g,\gamma_2,|\Omega_1|)$, R_R takes the form

$$R_R=\frac{\lambda_1^2}{8\pi N_Q}\gamma_e\langle Q_{ee}\rangle NL=\frac{\pi\hbar|d_{eg}|^2|\Omega_1|^2NL}{4\epsilon_0\Omega_e^2\lambda_1}, \tag{47}$$

where N_Q takes the value of 2 because of the linear polarizers placed before fiber coupling and $\langle Q_{ee}\rangle=2|\Omega_1|^2/(\gamma_e^2+4\Omega_e^2)$ is the population distributed in the excited state $|e\rangle$. In the second derivation we have used $\gamma_e=8\pi^2\hbar|d_{eg}|^2/\epsilon_0\lambda_1^3$ with $\lambda_1=2\pi c/\omega_1$. As we see in Eq. (47), the single-photon counting rate from the linear Rayleigh scattering (of the pump beam) is proportional to the pump power times the optical depth, but inversely proportional to the squared effective Rabi frequency. Recall that the efficiencies of two detectors are assumed to be 100%. The constant R_0 in Eq. (44) [and Eq. (45)] is

$$R_0 = \left(\frac{\hbar |d_{ge}|^2 |\Omega_1|^2 \omega_1 Q_0 NL}{4\pi c p_0 \Delta \Omega_e} \right)^2, \tag{48}$$

where Q_0 is given in Eq. (10) and may be approximated as unity. Therefore, from Eqs. (44) and (46)–(48), one can find that

$$g^{(2)}(\tau) = 1 + \left(\frac{2\sqrt{2}\Omega_e}{\pi\Delta} \right)^2 [\cosh(\Gamma_0 - \Gamma)\tau - \cos(\Omega_e \tau)] e^{-(\Gamma_0+\Gamma)\tau}, \tag{49}$$

where $\cosh(x)$ is a hyperbolic function. To obtain some insights in Eq. (49), let us look at the visibility, which is defined as

$$V_{\text{vis}} = \frac{g^{(2)}_{\max} - g^{(2)}_{\min}}{g^{(2)}_{\max} + g^{(2)}_{\min}},$$

where $g^{(2)}_{\max}$ and $g^{(2)}_{\min}$ correspond to the maximum and minimum of $g^{(2)}(\tau)$, respectively. From Eq. (49), at $\tau=0$ or $\tau=+\infty$, $g^{(2)}$ approaches the minimum at 1. The maximum can be numerically found by solving the transcendental equation. By examining Eq. (49), it is easy to find that the maximum in creases as well as the increase of the effective Rabi frequency (e.g., increasing the pump detuning) and vice versa. Therefore the maximum of $g^{(2)}$ is bounded in the range 1 to $1+2(2\sqrt{2}\Omega_e/\pi\Delta)^2$. Using the concept of the visibility given above, one can obtain

$$0 < V_{\text{vis}} < \frac{\left(\frac{2\sqrt{2}\Omega_e}{\pi\Delta} \right)^2}{1 + \left(\frac{2\sqrt{2}\Omega_e}{\pi\Delta} \right)^2}. \tag{50}$$

In the weak-optical-excitation case, Ω_e is approximated as Δ. The inequality in Eq. (50) is then simplified as

$$0 < V_{\text{vis}} < \frac{\left(\frac{2\sqrt{2}}{\pi} \right)^2}{1 + \left(\frac{2\sqrt{2}}{\pi} \right)^2} = 44.8\%. \tag{51}$$

As seen in Eq. (50), the visibility increases as well as increasing the ratio of Ω_e/Δ. The maximum of V_{vis} is limited to be below 45%. In the next subsection we will compare the results obtained above with the experimental ones.

Before the preceding, there is a simplified physical picture to understand the biphoton in the two-level system. Without including the linewidths of the triplet structure, the two-photon state can be written as $|\psi\rangle = |\delta=0, \delta=0\rangle - |\delta=-\Delta, \delta=\Delta\rangle$, where the first term characterizes the correlated photons generated from the central component and the second term indicates the paired photons generated from the two sidebands. The "−" sign indicates the phase difference between two types of processes shown in Fig. 2. The biphoton wave packet then becomes $\psi(t_1,t_2) = 1 - e^{i\Delta(t_1-t_2)}$. Therefore, the non-normalized temporal correlation is given by $|\psi(t_1,t_2)|^2 = 2[1-\cos\Delta(t_1-t_2)]$, which coincides with the essential result derived in Eq. (45).

B. Comparison between experiment and theory

Cold atoms with negligible Doppler broadening is a perfect source to study the biphoton generation in a two-level system. The experiments were done with cold ^{87}Rb atoms prepared by a standard six-beam magneto-optical trap (MOT) [24]. In the experiment done by Harris' group at Stanford [15], the pump laser, blue detuned Δ from the D2 line transition $|5S_{1/2}, F=2\rangle \rightarrow |5P_{3/2}, F'=3\rangle$, is linearly polarized and collimated to overlap the atomic cloud. The pump power was 770 μW with a detuning $2\pi \times 83.6$ MHz. The experimental data of the two-photon coincidence measurement are illustrated in Fig. 4(a) (from [15]). As we see, the coincidence counts show a damped Rabi oscillation. At the delay time $\tau=0$, the interference of contributions from the central component and sidebands in the triplet resonance structure leads to antibunching. The temporal width of the two-photon coincidence is more than 300 ns. The long tail is determined by γ_g as given in Eq. (44). The background coincidences are due to the linear Rayleigh scattering of the pump beam.

The comparison between theory and experiment is given in Fig. 4(b) where the red line (with smaller fluctuations) is the experimental data and the blue line (with higher fluctuations) is the theoretical simulation. Both theory and experiment show an agreement with each other. It was found that the oscillation period is indeed determined by the effective Rabi frequency $\Omega_e = \sqrt{\Delta^2 + |\Omega_1|^2}$. In the experiment, since the pump detuning ($\Delta = 2\pi \times 83.6$ MHz) is certainly greater than the Rabi frequency of the pump ($|\Omega_1| = 26$ MHz), the effective Rabi frequency Ω_e is dominated by the pump detuning Δ rather than by the Rabi frequency $|\Omega_1|$ of the pump beam. The damping rate is mainly determined by the linewidth of the central component of the triplet, γ_g. The parameters in the simulation were chosen as $\gamma_2 = \gamma_e/2$ and $\gamma_g = 0.15\gamma_e$. γ_g is obtained by considering the pump linewidth (~300 KHz), MOT temperature (~300 KHz), and inhomogeneous magnetic field broadening (~1.4 MHz). The visibility shown in the experiment is 31% and the theoretical prediction is 40%. The difference of the visibilities between theory and experiment is because, in the simulation, we did not consider the absorption and loss. When including the absorption and loss occurring in the atomic system, we can obtain a better agreement between theory and experiment [25]. (In [25], the coupled Maxwell's equations are solved for the two weak generated fields and the results also show an agreement with the experiment.)

To fit the experimental data using the obtained theory, we found that (1) as the pump power increases, both the dipole dephasing rate γ_2 and the linewidth of the ground state γ_g become greater and (2) the long tail background in the two-photon correlation measurements are due to the linewidth of the inhomogeneous-broadened ground state, γ_g.

To further verify the validity of the theory, it is necessary to recover the conventional input-output four-wave mixing in a two-level system. Suppose that in the input-output experiment, the field with the frequency ω_3, has an initial input. We measure the generated field at frequency ω_4 in the backward geometry, which gives

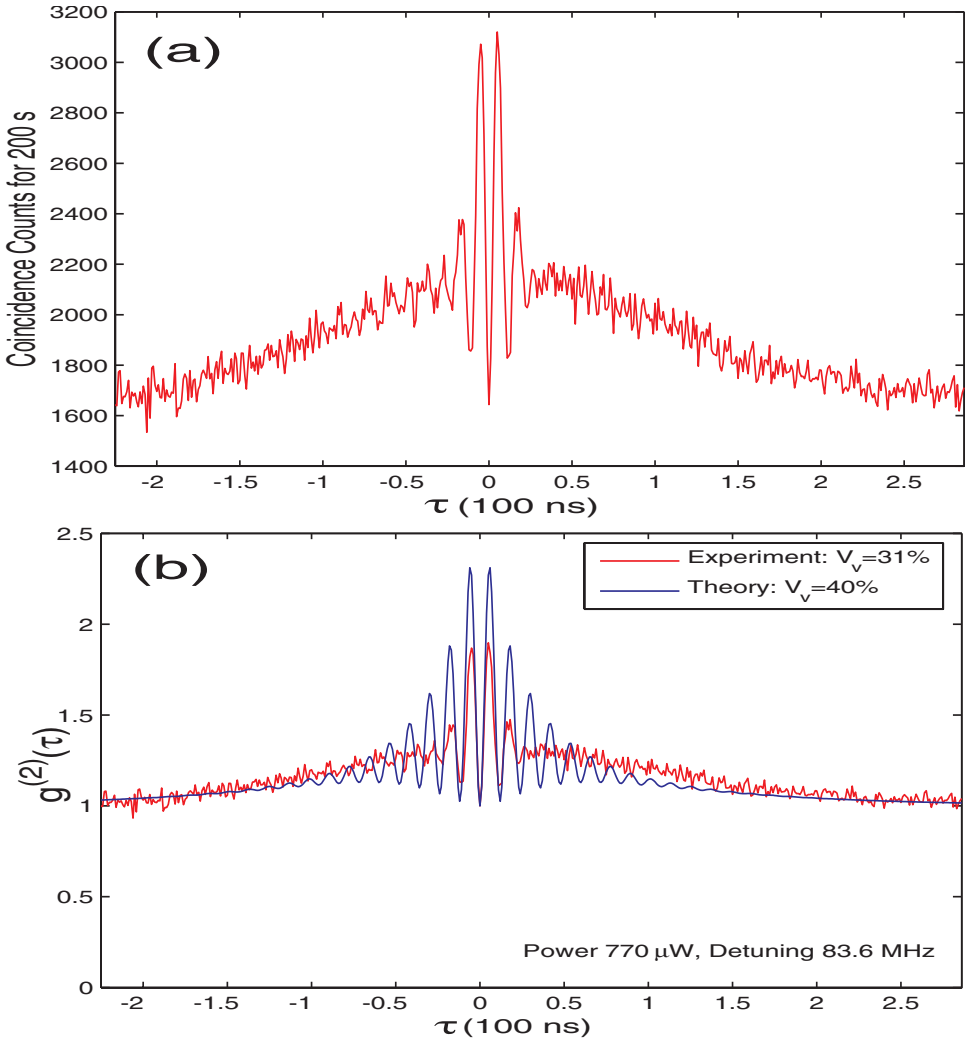

FIG. 4. (Color online) (a) Experiment: Coincidence counts as a function of the time delay between detected photons [15]. (b) Comparison of $g^{(2)}(\tau)$: The red line (with smaller fluctuations) is the experimental data and the blue line (with higher fluctuations) gives the theoretical simulation.

$$\langle E_4^{(-)} E_4^{(+)} \rangle = R \int d\delta |\chi_4^{(3)}(\delta)|^2. \tag{52}$$

$\chi_4^{(3)}(\delta)$ is the total susceptibility as given in Eq. (20) and R is a constant. In the above derivation, we have assumed that the input ω_3 field is very weak. Equation (52) is exactly the same as the conventional result [18]. The reason is that in such a measurement, which is the first-order coherence, the phase information is lost and the time-order is not detected.

V. SUMMARY

In summary, we have studied the nature of the two-photon state or biphoton created in an open two-level system. The comparison between theory and experiment shows a good agreement. To simplify the discussions we have assumed the idealized two-level medium and ignored the Doppler effect and quantum Langevin noise. In our simple model, we also ignore polarization effects. It was found that the two-photon bandwidth is mainly determined by the atomic linewidths, because the phase matching is satisfied over the entire atomic bandwidths. The temporal correlation measurement of the biphoton shows damped Rabi oscillations. The oscillation rate is determined by the effective Rabi frequency and the damping rate is determined by the linewidth of the central component of triplet resonances in a two-level system. The triplet resonances of a two-level system lead to two kinds of four-wave mixing processes. As shown in Eq. (44), the first term in brackets is the correlation due to the central resonant components, the second term stands for the correlation between sideband photons, and the third term is an interference. The interference in the two-photon coincidence measurement shows a photon antibunching-like effect. In Fig. 2(a), the correlations between photons may exhibit photon bunching as discovered by Hanbury-Brown and Twiss. In Fig. 2(b), correlated sideband photons are produced after absorbing two counter-propagating pump photons. In the large-detuning or strong pump case, the triplet resonances are well separated. In such a case, we can see the separated correlations from the central components or between sidebands by using proper filters [19]. The linear Rayleigh scattering of the pump beam provides the background noise in the experiment. There is no correlation between two photons, one from the central component and the other from one of the sidebands, in the second-order coherence. The visibility of the normalized second-order quantum coherence function $g^{(2)}(\tau)$ in such a two-level system increases along with the increase of the effective Rabi frequency, but has an upper limit at 45%.

ACKNOWLEDGMENTS

We wish to thank Y.-H. Shih, J. D. Franson, G. Y. Yin, and T. Pittman for stimulating discussions. We also thank Sulakshana Thanvantri, Giuliano Scarcelli, and Hai Zhang for help. J.-M.W. and M.H.R. were supported in part by the U.S. ARO MURI Grant No. W911NF-05-1-0197. S.D. acknowledges financial support from the Defense Advanced Research Projects Agency, the U.S. Air Force Office of Scientific Research, and the U.S. Army Research Office.

APPENDIX: THE SINGLE-PHOTON COUNTING RATE

To discuss the single-photon properties of the radiation, we consider an experiment such as that shown in Fig. 1(b) with detector D2 removed. The average counting rate is given by

$$R_s = \lim_{T\to\infty} \frac{1}{T}\int_0^T dt_a \langle \Psi | E_a^{(-)} E_a^{(+)} | \Psi \rangle. \tag{A1}$$

The second-order field correlation function in Eq. (A1) may be written as

$$\langle \Psi | E_a^{(-)} E_a^{(+)} | \Psi \rangle = \sum_{\vec{k}} |\langle 0 | a_{\vec{k}} E_a^{(+)} | \Psi \rangle|^2. \tag{A2}$$

Using Eq. (26), one can obtain

$$\langle 0 | a_{\vec{k}} E_a^{(+)} | \Psi \rangle = \sum_{\vec{k}_a} \sum_{\vec{k}_3} \sum_{\vec{k}_4} e^{-i\omega_a \tau_1} F(\vec{k}_3, \vec{k}_4) \delta_{\vec{k}_3 \vec{k}_a} \delta_{\vec{k}\vec{k}_4}. \tag{A3}$$

Substituting this into Eq. (A2) gives

$$\langle \Psi | E_a^{(-)} E_a^{(+)} | \Psi \rangle = \sum_{\vec{k}} \frac{V_Q}{(2\pi)^3} \left| \sum_{\vec{k}_3} e^{-i\omega_3 \tau_1} F(\vec{k}_3, \vec{k}) \right|^2. \tag{A4}$$

To simplify the calculation, we treat the transverse detuning function (29) as a δ function so that the wave vectors can be replaced by wave numbers. To evaluate the Dirac δ functions in $F(k_3, k)$, a summation over a wave number is converted into an angular frequency integral as given by Eq. (36). Then the single-photon counting rate (A1) becomes

$$R_s = R_{s0} \int d\delta \left| \chi_3^{(3)} \Phi\left(\frac{2\delta L}{v_3} \right) \right|^2. \tag{A5}$$

R_{s0} absorbs all the slowly varying terms and constants. As seen from Eq. (A5), the single-photon counting rate is independent of time as expected.

[1] A. Einstein, B. Podolsky, and N. Rosen, Phys. Rev. **47**, 777 (1935).

[2] E. Schrödinger, Naturwiss. **23**, 807 (1935); **23**, 823 (1935); **23**, 844 (1935) [translation in *Quantum Theory of Measurement*, edited by J. A. Wheeler and W. H. Zurek (Princeton University Press, Princeton, 1983)].

[3] D. Bohm, *Quantum Theory* (Prentice-Hall, Englewood Cliffs, NJ, 1951).

[4] I. Chuang and M. Neilson, *Quantum Computation and Quantum Information* (Cambridge University Press, Cambridge, England, 2000).

[5] A. V. Belinskii and D. N. Klyshko, J. Exp. Theor. Phys. **78**, 259 (1994); P. H. S. Ribeiro, S. Padua, J. C. MachadodaSilva, and G. A. Barbosa, Phys. Rev. A **49**, 4176 (1994).

[6] A. N. Boto, P. Kok, D. S. Abrams, S. L. Braunstein, C. P. Williams, and J. P. Dowling, Phys. Rev. Lett. **85**, 2733 (2000); M. D'Angelo, M. V. Chekhova, and Y. Shih, *ibid.* **87**, 013602 (2001).

[7] D. Bouwmeester, A. Ekert, and A. Zeilinger, *The Physics of Quantum Information* (Springer-Verlag, Berlin, 2000); A. Migdall, R. Datla, A. V. Segienko, J. S. Orszak, and Y.-H. Shih, Appl. Opt. **37**, 3455 (1998).

[8] B. E. A. Saleh, B. M. Jost, H.-B. Fei, and M. C. Teich, Phys. Rev. Lett. **80**, 3483 (1998).

[9] M. H. Rubin, D. N. Klyshko, Y.-H. Shih, and A. V. Sergienko, Phys. Rev. A **50**, 5122 (1994); D. N. Klyshko, *Photons and Nonlinear Optics* (Gordon and Breach Science, New York, 1988).

[10] M. H. Rubin, Phys. Rev. A **54**, 5349 (1996); Y.-H. Shih, Rep. Prog. Phys. **66**, 1009 (2003); L. Mandel, Rev. Mod. Phys. **71**, S274 (1999); A. Zeilinger, *ibid.* **71**, S288 (1999).

[11] S. E. Harris, Phys. Today **50**, 36 (1997); M. D. Lukin, Rev. Mod. Phys. **75**, 457 (2003); M. Fleischhauer, A. Imamoglu, and J. Marangos, *ibid.* **77**, 633 (2005).

[12] A. Kuzmich, W. P. Bowen, A. D. Boozer, A. Boca, C. W. Chou, L.-M. Duan, and H. J. Kimble, Nature (London) **423**, 731 (2003).

[13] C. H. van der Wal, M. D. Eisaman, A. André, R. L. Walsworth, D. F. Phillips, A. S. Zibrov, and M. D. Lukin, Science **301**, 196 (2003).

[14] V. Balić, D. A. Braje, P. Kolchin, G. Y. Yin, and S. E. Harris, Phys. Rev. Lett. **94**, 183601 (2005).

[15] P. Kolchin, S. Du, C. Belthangady, G. Y. Yin, and S. E. Harris, Phys. Rev. Lett. **97**, 113602 (2006).

[16] J. K. Thompson, J. Simon, H. Loh, and V. Vuletić, Science **313**, 74 (2006).

[17] J.-M. Wen and M. H. Rubin, Phys. Rev. A **74**, 023808 (2006); **74**, 023809 (2006); P. Kolchin (unpublished); L.-M. Duan, M. D. Lukin, J. I. Cirac, and P. Zoller, Nature (London) **414**, 413 (2001); M. O. Scully and C. H. R. Ooi, J. Opt. B: Quantum Semiclassical Opt. **6**, S816 (2004).

[18] R. W. Boyd, *Nonlinear Optics* (Academic Press, San Diego, CA, 1992); R. W. Boyd, M. G. Raymer, P. Narum, and D. J. Harter, Phys. Rev. A **24**, 411 (1981).

[19] P. Grangier, G. Roger, A. Aspect, A. Heidmann, and S. Reynaud, Phys. Rev. Lett. **57**, 687 (1986); A. Aspect, G. Roger, S. Reynaud, J. Dalibard, and C. Cohen-Tannoudji, *ibid.* **45**, 617 (1980); J. Dalibard and S. Reynaud, J. Phys. (Paris) **44**, 1337 (1983).

[20] M. W. Mitchell, C. I. Hancox, and R. Y. Chiao, Phys. Rev. A **62**, 043819 (2000).

[21] See R. Loudon, Phys. Bull. **27**, 21 (1976), reprinted in L.

Allen and P. L. Knight, *Concepts of Quantum Optics* (Oxford Press, Pergamon, 1983); D. F. Walls, Nature (London) **280**, 451 (1979); H. Paul, Rev. Mod. Phys. **54**, 1061 (1982).

[22] J.-M. Wen, M. H. Rubin, and S. Du (unpublished). In this paper, the Langevin noise operators are carefully addressed by analyzing the second-order quantum coherence function.

[23] H. Hanbury-Brown and R. Q. Twiss, Philos. Mag. **45**, 663 (1954); Nature (London) **178**, 1046 (1956); Proc. R. Soc. London, Ser. A **242**, 300 (1957).

[24] E. L. Raab, M. Prentiss, Alex Cable, Steven Chu, and D. E. Pritchard, Phys. Rev. Lett. **59**, 2631 (1987).

[25] S. Du, J.-M. Wen, M. H. Rubin, and G. Y. Yin, Phys. Rev. Lett. **98**, 053601 (2007).